REFERENCES AND NOTES

1. G. Binnig, C. F. Quate, Ch. Gerber, *Phys. Rev. Lett.* **56**, 930 (1986).
2. P. K. Hansma, V. B. Elings, O. Marti, C. E. Bracker, *Science* **242**, 209 (1988).
3. G. Binnig, Ch. Gerber, E. Stoll, T. R. Albrecht, C. F. Quate, *Europhys. Lett.* **3**, 1281 (1987).
4. T. R. Albrecht and C. F. Quate, *J. Appl. Phys.* **62**, 2599 (1987).
5. T. R. Albrecht *et al.*, *ibid.* **64**, 1178 (1988).
6. C. M. Mate, G. M. McClelland, R. Erlandsson, S. Chiang, *Phys. Rev. Lett.* **59**, 1942 (1987).
7. Y. Martin and H. K. Wickramasinghe, *Appl. Phys. Lett.* **50**, 1455 (1987).
8. S. Alexander *et al.*, *J. Appl. Phys.* **65**, 164 (1989).
9. B. Drake *et al.*, *Science* **243**, 1586 (1989).
10. D. D. Lee, *J. Cryst. Growth* **102**, 262 (1990); L. Pach *et al.*, *J. Mater. Res.* **5**, 2928 (1990); S. Mann, *Nature* **332**, 119 (1988); _____, B. R. Heywood, S. Rajam, J. D. Birchall, *ibid.* **334**, 692 (1988); L. Addadi and S. Weiner, *Proc. Natl. Acad. Sci. U.S.A.* **82**, 4110 (1985); A. Berman, L. Addadi, S. Weiner, *Nature* **331**, 546 (1988); A. Berman *et al.*, *Science* **250**, 664 (1990); J. D. Birchall, *Trans. J. Br. Ceram. Soc.* **83**, 158 (1984).
11. Digital Instruments, 6780 Cortona Drive, Santa Barbara, CA 93117.
12. D. Rugar and P. Hansma, *Phys. Today* **43** (no. 10), 23 (1990).
13. J. A. C. Nicol, *The Biology of Marine Animals* (Interscience, New York, 1960), p. 646.
14. H. R. Wenk, D. J. Barber, R. J. Reeder, in *Reviews in Mineralogy*, R. J. Reeder, Ed. (Mineralogical Society of America, Washington, DC, 1983), vol. 11, pp. 301–367; F. Dachille and R. Roy, *Nature* **186**, 34 (1960); J. H. Burns and M. A. Bredig, *J. Chem. Phys.* **25**, 1281 (1956); R. Schrader and Br. Hoffmann, *Z. Chem.* **6**, 388 (1966).
15. Simulations were done with Chem-X, developed and distributed by Chemical Design Ltd., Oxford, England. The simulations were constructed based on published x-ray diffraction parameters (lattice parameters, atomic coordinates, and space groups). Crystallographic parameters for simulating the aragonite structure were from A. Dal Negro and L. Ungaretti, *Am. Mineral.* **56**, 768 (1971). Those for the calcite structure were from H. Chessin and W. C. Hamilton, *Acta Crystallogr.* **18**, 689 (1965).
16. Support of this work by the National Science Foundation, Solid State Physics grants no. DMR 89-17164 (P.K.H.) and no. DMR 88-21499 (G.D.S.), the Austrian Fonds zur Förderung der Wissenschaftlichen Forschung (G.F.), and Concrete Technology Corp. (E.R. and G.D.S.) is gratefully acknowledged. Purchases and building of AFM equipment were supported in part by the Office of Naval Research and Digital Instruments.

11 February 1991; accepted 10 July 1991

The Dark Side of Venus: Near-Infrared Images and Spectra from the Anglo-Australian Observatory

D. CRISP,* D. A. ALLEN, D. H. GRINSPOON,† J. B. POLLACK

Near-infrared images and spectra of the night side of Venus taken at the Anglo-Australian Telescope during February 1990 reveal four new thermal emission windows at 1.10, 1.18, 1.27, and 1.31 micrometers (μm), in addition to the previously discovered windows at 1.74 and 2.3 μm. Images of the Venus night side show similar bright and dark markings in all windows, but their contrast is much lower at short wavelengths. The 1.27-μm window includes a bright, high-altitude O_2 airglow feature in addition to a thermal contribution from the deep atmosphere. Simulations of the 1.27- and 2.3-μm spectra indicate water vapor mixing ratios near 40 ± 20 parts per million by volume between the surface and the cloud base. No large horizontal gradients in the water vapor mixing ratios were detected at these altitudes.

ALLEN AND CRAWFORD (*1*) DISCOVered that the night side of Venus is surprisingly bright at near-infrared (NIR) wavelengths between 1 and 3 μm. Their spectroscopic measurements revealed emission peaks near 1.74 and 2.3 μm, in the relatively transparent spectral windows between CO_2 and H_2O absorption bands in the Venus atmosphere, where the planet-wide sulfuric acid (H_2SO_4) clouds provide the principal source of opacity. NIR images of the night side of Venus show bright and dark markings that move from east to west with rotation periods between 5 and 7 days. This night-side emission is produced by hot gases in the lower atmosphere of Venus, below the H_2SO_4 cloud deck (*2, 3*). The NIR markings are formed as this radiation passes through regions of the clouds that have different optical depths (*3*).

Analyses of NIR spectra have provided improved estimates of the concentrations of important trace gases in the deep atmosphere including H_2O, HDO, CO, and OCS (*4, 5*). Most NIR spectra (*2, 4, 5*) indicate water vapor mixing ratios near 40 parts per million by volume (ppmv) at altitudes between 30 and 50 km. Only one NIR spectrum (*5*) indicates much larger amounts of water (200 ppmv) similar to those inferred from entry probe measurements (*6, 7*). The limited spatial sampling provided by these NIR spectra does little to constrain the global distribution of H_2O below the clouds, but, if the dry conditions indicated by most of these spectra prevail throughout the deep atmosphere, they have important implications for the atmospheric evolution and the efficiency of the greenhouse mechanism that maintains the high surface temperatures. Comparisons between the H_2O and HDO abundances derived from NIR spectra confirm that the Venus atmosphere has lost a substantial amount of H_2O since its formation (*4*). With such losses, small H_2O amounts similar to those detected in most NIR spectra may have atmospheric lifetimes shorter than the age of the solar system (*8*). These arguments suggest that the present H_2O amounts may be maintained by a steady-state influx from volcanoes or comets. They also preclude the need for a large primordial water inventory. This, in turn, weakens current theories on the origin and evolution of the massive CO_2 atmosphere and the high surface temperatures on Venus, because large H_2O amounts play a vital role in the primordial "runaway greenhouse" that is thought to have produced these conditions (*9*).

These NIR observations also raise questions about the present-day greenhouse

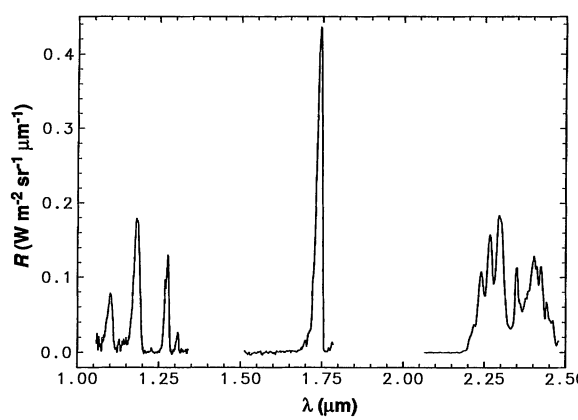

Fig. 1. Radiance R plotted as a function of wavelength λ for a low-resolution spectrum ($\lambda/\Delta\lambda \sim 600$) of a bright region on the night side of Venus from 10 February 1990. The new thermal emission windows at 1.10, 1.18, 1.27, and 1.31 μm are shown as well as the previously discovered 1.74- and 2.3-μm features.

D. Crisp, MS 169-237, Jet Propulsion Laboratory, California Institute of Technology, 4800 Oak Grove Drive, Pasadena, CA 91109.
D. A. Allen, Anglo-Australian Observatory, Post Office Box 296, Epping, New South Wales, 2121, Australia.
D. H. Grinspoon and J. B. Pollack, MS 245-3, National Aeronautics and Space Administration (NASA) Ames Research Center, Moffett Field, CA 94035.

*To whom correspondence should be addressed.
†Present address: Laboratory for Atmospheric and Space Physics, University of Colorado, Boulder, CO 80309.

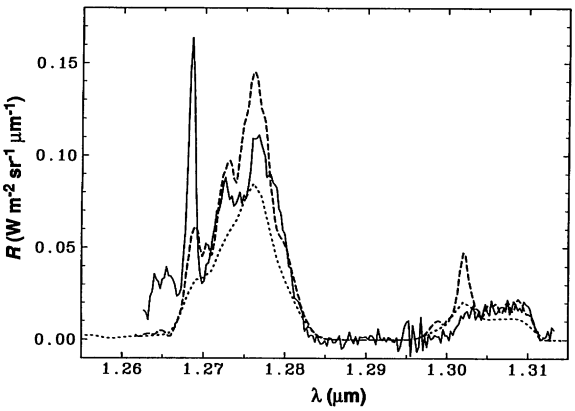

Fig. 2. A high-resolution spectrum ($\lambda/\Delta\lambda \sim 1280$) of the new windows at 1.27 and 1.31 μm taken on 13 February 1990 by centering the 1.4–arc sec aperture of FIGS on a bright region (solid line). At this resolution, the slowly varying thermal contribution is clearly separated from the sharp O_2 ($^1\Delta_g$) airglow feature at 1.269 μm, but the individual lines that compose the O_2 feature are not resolved. Simulations for bright-spot (long dash) and dark-spot (dotted line) cloud models are also shown. All of the mode 2′ and 3 cloud particles were omitted from the bright-spot model to maximize the contrast. The O_2 ($^1\Delta_g$) emission was intentionally omitted from the simulations.

mechanism. Both water vapor and H_2SO_4 aerosols are essential components of this greenhouse because they prevent thermal radiation from escaping through atmospheric windows between strong CO_2 bands. Successful simulations of the high surface temperatures on Venus (*10*) require large H_2O mixing ratios (100 to 1000 ppmv) and a thick, unbroken cloud deck. The smaller H_2O vapor abundances and the partial clearings in the H_2SO_4 clouds revealed by these NIR observations indicate that other greenhouse agents, or other radiative processes that were not included in those models, are needed to account for the high surface temperatures. Because the low H_2O mixing ratios derived from these NIR spectra have raised such profound questions about the Venus atmosphere, improved estimates of the global abundance and spatial distribution of this gas are essential. In addition, spatial maps of other trace gases that have been detected in NIR spectra, including CO and OCS (*4*), could provide valuable constraints on the atmospheric chemistry and vertical transport in the Venus atmosphere.

A broad range of new NIR spectroscopic and imaging observations of Venus was conducted from a global network of ground-based telescopes in conjunction with the Galileo spacecraft's flyby of Venus in February 1990. In this paper, we report the observations that were taken with the Fabry-Perot infrared grating spectrometer (FIGS) (*11*) mounted on the 3.9-m Anglo-Australian Telescope (AAT). Unlike the earlier spectroscopic studies that focused on the 1.7- and 2.3-μm windows (*2, 4, 5*), this program included observations at shorter wavelengths as well. Four new spectral windows were discovered at 1.10, 1.18, 1.27, and 1.31 μm (*12*) (Figs. 1 and 2). These new windows allow thermal radiation to escape from lower altitudes than the previously discovered 1.7- and 2.3-μm windows and provide opportunities to study the abundances of H_2O and other trace gases in the lowest scale height (<20 km) of the Venus atmosphere. New spectra were taken in the 1.7- and 2.3-μm windows (Fig. 3) to determine the amounts of H_2O, CO, and OCS just below the cloud base (25 to 47 km) and to facilitate comparisons with earlier observations (*2, 4, 5*). In addition to these spectra of isolated regions of the Venus night side, we scanned the spectrometer across the planet to construct spectral image cubes (*13*) consisting of full-disk images at 16 discrete wavelengths within the telluric J (1.3 μm), H (1.7 μm), and K (2.2 μm) windows (Fig. 4). These image cubes place improved constraints on the mechanisms that produce the NIR markings and the spatial distributions of trace gases below the Venus cloud deck.

Two theoretical radiative transfer algorithms were used to analyze these observations. The first (*5, 14*) was used primarily to study the 2.3-μm spectra. The second (*15*) was used for the new shortwave windows near 1.18, 1.27, and 1.31 μm. Both models are based on line-by-line (monochromatic) solutions to the equation of transfer that explicitly include absorption, emission, and multiple scattering by CO_2, H_2O, CO, OCS, and the H_2SO_4 cloud particles. The multiple scattering algorithms used in these models occasionally produce absolute intensity errors as large as 10%, but relative (wavelength to wavelength) errors are usually much smaller. Much larger errors were introduced by uncertainties in the NIR optical properties of CO_2, H_2O, OCS, and SO_2 at high temperatures and pressures. Available absorption line databases such as HITRAN (*16*) are not sufficiently accurate or complete for Venus applications (*4*). We therefore augmented the HITRAN line listings near 2.3 μm with information from a variety of sources (*17*). For the new spectral windows at shorter wavelengths, the HITRAN CO_2 database was replaced entirely with a new high-temperature CO_2 database recently developed by Wattson (*18*). This database includes many more (>600) weak overtone bands and hot bands that produce significant opacity in the deep atmosphere of Venus.

Pressure and temperature profiles from the Venus International Reference Atmosphere (VIRA) were used in all simulations (*19*). The CO_2 volume mixing ratio was 0.965 at all levels. Initial estimates of mixing ratios for H_2O, CO, and OCS were taken from Bezard *et al.* (*4*). The H_2SO_4 aerosol distributions were based on cloud models compiled from Pioneer Venus and Venera entry probe measurements (*20*). We modi-

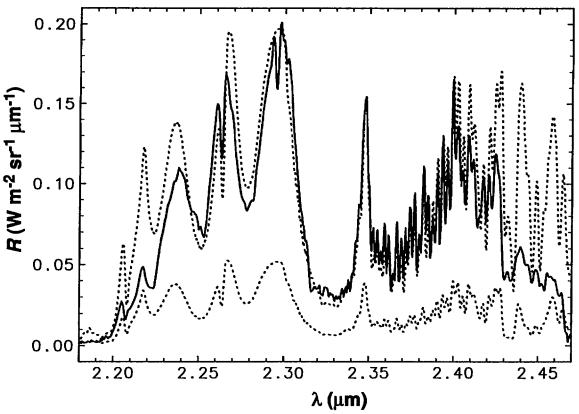

Fig. 3. High-resolution spectrum ($\lambda/\Delta\lambda \sim 1150$) of the 2.3-μm window taken on 10 February 1990 by centering the 1–arc sec aperture of FIGS on a bright region in the northern hemisphere of the Venus night side (solid line). This radiation is emitted primarily by the far wings of pressure-broadened CO_2 and H_2O lines at levels between the cloud base (1.5 bars, ~47 km) and the 8-bar level (~32 km). The short wavelength side of this window is defined by weak CO_2 bands. Both H_2O and CO_2 bands produce extinction on the long wavelength side. H_2O and HDO are the principal absorbers near 2.4 μm. The strong absorption feature occupying the central third of the 2.3-μm window is the CO (2-0) band. The $2\nu_3$ band of OCS is responsible for the feature near 2.45 μm (*4*). Simulations for bright-spot (upper dotted line) and dark-spot (lower dotted line) cloud models are also shown. We created a best-fit bright-spot model by removing 53% of the mode 2′ and mode 3 particles from the middle and lower clouds. The discrepancies on the shortwave side of the 2.3-μm window are caused by errors in the CO_2 database. Errors at wavelengths longer than 2.43 μm are caused primarily by errors and omissions in our OCS and SO_2 line listings. Variations in the telluric water vapor abundance during our observations may also contribute to discrepancies at these wavelengths.

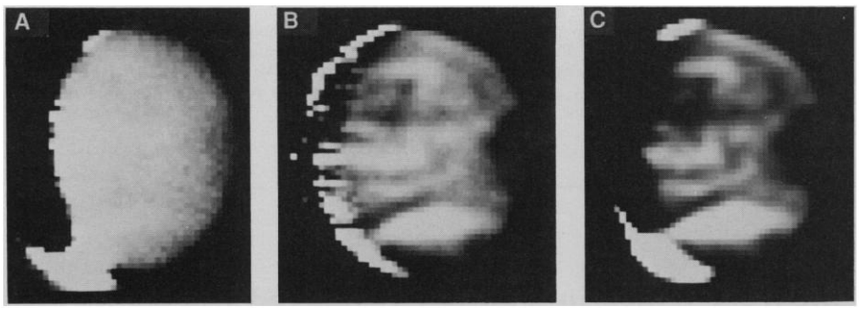

Fig. 4. Images of the Venus night side in the (**A**) J (1.3 μm), (**B**) H (1.7 μm), and (**C**) K (2.2 μm) windows taken on 13 February 1990. They all show similar markings, but the contrast between dark and bright markings increases with wavelength.

fied these cloud models by varying the particle number densities in the middle and lower clouds to match the observed night-side radiances. Two different cloud particle distributions were used in the simulations presented here. The nominal cloud structure described by Crisp (*20*) was adopted for the dark-spot simulation. We created alternate bright-spot models by reducing the optical depths of the clouds in the nominal model to simulate particle sedimentation and sublimation (*3*).

The broad spectral range included in these observations (1.1 to 2.5 μm) provides a more rigorous test of the hypothesis that the NIR markings are produced by horizontal variations in the optical depths of the H_2SO_4 clouds than was possible before (*2, 3*). The contrast between dark and bright markings increases from less than 0.3 at 1.27 μm, to more than 5 at 2.3 μm (Fig. 4). We could simulate these contrasts throughout this wavelength range by varying the optical depths of the clouds. We could not simulate them by altering the mixing ratios of H_2O, HDO, CO, or OCS. Our calculations were not particularly sensitive to the altitude range in which the optical depths of the clouds were changed, but they were sensitive to the sizes of the particles that were varied. We found that 50 to 60% variations in the optical depths of the largest particle modes in the middle and lower clouds (modes 2′ and 3) produced wavelength-dependent contrasts that are consistent with the observations (Fig. 4). Variations in the optical depths of other particle modes produced much smaller (modes 1 and 2) or much larger (mode 3 only) wavelength-dependent contrast variations. Differences in the optical depths of the clouds produce larger NIR contrasts at wavelengths near 2.3 μm because the H_2SO_4 aerosols are more absorbing there. The largest cloud particles (modes 2′ and 3) have a larger impact on the contrast near 2.3 μm because they have larger extinction cross sections and smaller single scattering albedos than the smaller particles.

Simulations of the high-resolution 1.27-μm spectrum (Fig. 2) confirm that it includes a large thermal contribution from the lowest scale height of the Venus atmosphere (0 to 20 km), as well as from the bright (>1 megarayleigh) O_2 ($^1\Delta_g$) airglow feature at 1.269 μm, which is produced above the cloud tops at altitudes near 100 km (*21*). The intensity of this airglow has puzzled atmospheric chemists for more than a decade. Parisot and Moreels (*22*) attributed the O_2 ($^1\Delta_g$) airglow to ozone photolysis at levels between 90 and 100 km on the day side of Venus, but their model underestimates the intensity of this feature by a factor of 10. Yung and Demore (*23*) found that reactions involving HO_x and NO_x were also exothermic enough to contribute to the population of this excited state of O_2, but their model could account for less than half of the observed airglow. More comprehensive photochemical models of this part of the Venus atmosphere are apparently needed to account for the observed abundance of O_2 ($^1\Delta_g$) above the Venus clouds.

Simulations of the 1.27- and 2.3-μm spectra (Figs. 2 and 3) indicate that the H_2O mixing ratio is 40 ± 20 ppmv at altitudes between the surface and the cloud base. These values are consistent with H_2O mixing ratios derived from most other NIR spectra (*2, 4*), but they are only 5 to 40% as large as those measured by Bell *et al.* (*5*), or by the Pioneer Venus (*6*) and Venera (*7*) entry probes. The CO and OCS abundances in the deep atmosphere are similar to those derived by Bezard *et al.* (*4*). The primary source of uncertainty in our estimates of the H_2O, CO, and OCS abundances arises from deficiencies in the NIR absorption parameters for CO_2 and H_2O at high temperatures and pressures. Both improved laboratory measurements and more sophisticated quantum-mechanical models of these molecules are required to take full advantage of these and future NIR spectra of Venus.

To determine the spatial distributions of H_2O, CO, and OCS near the cloud base (30 to 45 km), we constructed absorption maps from the K-band image cubes. H_2O is the principal absorbing gas near 2.4 μm, but it absorbs very little near 2.3 μm (*4, 5*). The H_2SO_4 clouds have comparable effects at both wavelengths. Ratios of 2.3- and 2.4-μm images therefore show little evidence of the NIR markings, but H_2O variations as large as those reported by Bell *et al.* should appear as factor of 2 contrast differences. H_2O maps constructed from images taken on 13 February 1990 show no contrast differences on the night side that are above the noise level (10%). CO and OCS maps also show no large contrasts. We therefore conclude that the lower atmosphere of Venus was relatively dry and that the H_2O was uniformly distributed. These observations do not completely preclude the much wetter conditions reported earlier because our maps refer to only a single day and describe less than 30% of the planet. A more comprehensive NIR monitoring program is needed to determine the spatial and temporal dependence of the H_2O budget in the Venus atmosphere.

REFERENCES AND NOTES

1. D. A. Allen and J. W. Crawford, *Nature* **307**, 222 (1984).
2. D. A. Allen, *Icarus* **69**, 221 (1986); L. Kamp and F. W. Taylor, S. B. Calcutt, *Nature* **336**, 360 (1988); L. W. Kamp and F. W. Taylor, *Icarus* **86**, 510 (1990).
3. D. Crisp *et al.*, *Science* **246**, 506 (1989).
4. B. Bezard *et al.*, *Nature* **345**, 508 (1990); C. De Bergh *et al.*, *Science* **251**, 547 (1991).
5. J. F. Bell *et al.*, *Bull. Am. Astron. Soc.* **22**, 1052 (1990); J. F. Bell *et al.*, *Science* **252**, 1293 (1991).
6. J. H. Hoffman *et al.*, *J. Geophys. Res.* **85**, 7882 (1980); V. I. Oyama *et al.*, *ibid.*, p. 7891.
7. V. I. Moroz, in *Venus*, D. M. Hunten, L. Colin, T. M. Donahue, V. I. Moroz, Eds. (Univ. of Arizona Press, Tucson, 1983), pp. 45–68.
8. D. H. Grinspoon, *Science* **238**, 1702 (1987).
9. A. P. Ingersoll, *J. Atmos. Sci.* **26**, 1191 (1969); J. B. Pollack, *Icarus* **14**, 295 (1971); J. F. Kasting, *ibid.* **74**, 472 (1988).
10. J. B. Pollack, O. B. Toon, R. Boese, *J. Geophys. Res.* **85**, 8223 (1980).
11. J. Bailey *et al.*, *Publ. Astron. Soc. Pac.* **100**, 1178 (1988). The FIGS spectrometer has 16 InSb focal plane detectors spaced at intervals of six times their width. FIGS was mounted at the Cassegrain focus of the 3.9-m Anglo-Australian Telescope and used with the *f*/36 chopping secondary. We obtained high-resolution spectra by moving the diffraction grating in steps while keeping the spectrometer's entrance aperture at a fixed point on Venus. All observations were taken in daylight. We eliminated scattered light from the sun and thermal emission from Earth's atmosphere from the Venus spectra by subtracting a spectrum of a nearby region of sky from the Venus spectrum. We reduced scattered light from the bright sunlit crescent of Venus by subtracting an appropriately scaled spectrum of the crescent from each night-side spectrum.
12. D. Allen, *Int. Astron. Union Circ. 4962* (1990).
13. We produced the FIGS images by scanning the focal plane of the telescope across the 2.1 arc sec square entrance aperture of the spectrometer while holding the diffraction grating fixed. We accomplished the scanning in right ascension (east-west) by driving the chopping secondary in steps synchronized to the data recording. We achieved the scanning in declination (north-south)

by stepping the telescope at the end of each right ascension scan. A 2.1–arc sec square aperture was used for mapping, but the step size was 1 arc sec in both directions to provide Nyquist sampling. Several successive scans of the planet were made and subsequently added together to improve the signal-to-noise ratio. The sky brightness and the different zero points of the 16 detectors were estimated from measurements of the sky in the corners of each image and subtracted from the images. To reduce the effects of scattered sunlight from the bright crescent, we subtracted an appropriately scaled out-of-band image, taken at a wavelength where the Venus night side produces little radiation.

14. The first model was identical to that described by Bell *et al.* (*5*). The δEddington/Adding algorithm was used to solve the equation of transfer in an absorbing, emitting, scattering atmosphere [D. Crisp, *Icarus* **67**, 484 (1986)]. Monochromatic gas absorption coefficients were computed on a 0.01 cm^{-1} grid with a modified version of the line-by-line model described by D. Crisp [*J. Geophys. Res.* **95**, 14577 (1990)]. The model atmosphere was divided into 50 vertical layers between the surface and 100 km.
15. The second model was developed by B. Dalton at NASA Ames Research Center. It is based on a two-stream source function solution to the equation of transfer [O. B. Toon, J. B. Pollack, C. Sagan, *Icarus* **30**, 663 (1977); O. B. Toon, C. P. McKay, T. P. Ackerman, K. Santhanam, *J. Geophys. Res.* **94**, 16287 (1989)] and uses monochromatic gas absorption coefficients from FASTCODE [S. A. Clough, F. X. Kneizys, L. S. Rothman, W. O. Gallery, *SPIE* **277**, *Atmospheric Transmission*, 152 (1981)]. The spectral resolution was 0.1 cm^{-1}. The model atmosphere was divided into 22 vertical layers.
16. L. Rothman *et al.*, *Appl. Opt.* **26**, 4085 (1987); N. Husson *et al.*, *Ann. Geophys.* **4**, 185 (1986).
17. For CO_2, we adopted an approach similar to that described by Bezard *et al.* (*4*) and augmented the line parameters on the 1986 version of the HITRAN database with weaker transitions listed by L. S. Rothman [*Appl. Opt.* **25**, 1795 (1986)]. The band parameters for H_2O and CO were taken directly from the HITRAN database. The spectral line parameters for the OCS $2\nu_3$ band at 2.45 μm were taken from L. R. Brown *et al.*, *ibid.* **26**, 5154 (1987)]. In addition, we included collision-induced absorption by CO_2 by combining the absorption coefficients given by J. F. Moore [*Rep. X-630-72-48* (NASA Goddard Space Flight Center, Greenbelt, MD, 1971)] with a wavelength-independent component of 4×10^{-8} cm^{-1} $amagat^{-2}$. The latter source of continuum opacity was needed to produce an adequate fit to the shape of the spectrum at wavelengths between 2.15 and 2.3 μm, where CO_2 and the H_2CO_4 cloud particles are the only known sources of extinction. It has no known theoretical justification, but it may compensate for errors introduced by uncertainties in the shapes of the far wings of CO_2 lines or other factors.
18. The new database was constructed from solutions to the quantum mechanical equations based on the direct numerical diagonalization (DND) technique [R. B. Wattson and L. S. Rothman, *J. Mol. Spectrosc.* **119**, 83 (1986)]. The DND method yields line positions that are accurate to a 0.01 cm^{-1} and line intensities with accuracies exceeding 10%.
19. A. Seiff, in *Venus*, D. M. Hunten, L. Colin, T. M. Donahue, V. I. Moroz, Eds. (Univ. of Arizona Press, Tucson, 1983), pp. 215–279.
20. D. Crisp, *Icarus* **67**, 484 (1986). The main cloud deck consists of upper (57 to 70 km), middle (49 to 57 km), and lower (47 to 49 km) layers, each containing mixtures of H_2SO_4 droplets with the four distinct particle size populations described by R. G. Knollenberg and D. M. Hunten [*J. Geophys. Res.* **85**, 8039 (1980)]: mode 1 (0.3 μm), mode 2 (1.0 μm), mode 2′ (1.4 μm), and mode 3 (3.6 μm). The numbers in parentheses give the modal particle radius. A Mie-scattering model (J. B. Pollack *et al.*, *ibid.*, p. 8141) was used to derive the wavelength-dependent optical properties of each particle mode from the optical constants of liquid H_2SO_4 [K. F. Palmer and D. Williams, *Appl. Opt.* **14**, 208 (1975)]. Log-normal size distributions were used for all modes.
21. P. J. Connes *et al.*, *Astrophys. J.* **233**, L29 (1979).
22. J.-P. Parisot and G. Moreels, *Icarus* **42**, 46 (1980).
23. Y. L. Yung and W. B. Demore, *ibid.* **51**, 199 (1982).
24. This work was funded in part by grants from the NASA Planetary Astronomy and Planetary Atmospheres Programs to the Jet Propulsion Laboratory, California Institute of Technology, and the NASA Ames Research Center. Much of the computer time was provided by the Wide-Field–Planetary Camera II Project at the Jet Propulsion Laboratory. We thank B. Dalton for developing and assisting in the use of the computer program for the second model (*15*) and for running some of the simulations presented here. We thank the AAT Time Allocation Committee for awarding the observing time for this program.

19 March 1991; accepted 21 June 1991

Climatic Change in Tasmania Inferred from a 1089-Year Tree-Ring Chronology of Huon Pine

EDWARD COOK, TREVOR BIRD, MIKE PETERSON, MIKE BARBETTI, BRENDAN BUCKLEY, ROSANNE D'ARRIGO, ROGER FRANCEY, PIETER TANS

A climatically sensitive huon pine tree-ring chronology from western Tasmania allows inferences about Austral summer temperature change since A.D. 900. Since 1965, huon pine growth has been unusually rapid for trees that are in many cases over 700 years old. This growth increase correlates well with recent anomalous warming in Tasmania on the basis of instrumental records and supports claims that a climatic change, perhaps influenced by greenhouse gases, is in progress. Although this temperature increase exceeds any that are inferred to have occurred during the past 1089 years at this location, it has not yet clearly emerged from the natural background variability of climate in this part of the Southern Hemisphere.

COMPARED TO THE INSTRUMENTAL and historical climate records of the Northern Hemisphere (*1*), the Southern Hemisphere has relatively few high-resolution climatic time series that extend back more than 100 years (*2*). Yet, to evaluate properly recent climatic trends and fluctuations, especially for changes that might be induced by radiatively active trace gases, much longer records are needed (*3*). To help fulfill this need, we developed a climatically sensitive tree-ring chronology from Tasmania that extends back to A.D. 900.

The tree-ring site is a disjunct, subalpine stand of huon pine (*Lagarostrobus franklinii* C. J. Quinn) located at 950-m elevation on Mount Read, a 1124-m-high massif located in western Tasmania (Fig. 1) that projects above the local timberline. In all, 56 radii from 23 trees were sampled and processed for tree-ring analysis with the use of established methods (*4, 5*). After cross-dating and measurement, the ring-width series were standardized (*6*) to remove long-term growth trends attributed to increasing tree size and maturation. This approach was taken in order to avoid removing any long-term climatic variance that was potentially distinguishable from purely biological growth trends. We then averaged the standardized tree-ring indices using a robust mean to discount the influence of outliers (*6*). The result was a mean site chronology that covered the interval A.D. 900 to 1988 (Fig. 2).

Both very poor and very rapid growth periods have occurred over the past 100 years in the huon pine chronology. Growth was poor from 1898 to about 1913; four of the nine poorest years of accumulated growing degree-days since 1870 in Canterbury, New Zealand (*7*), occurred during this period, and it overlaps with part of the coldest period (1900 to 1935) in recorded New Zealand history (*8*). It also coincides with the occurrence of a cold sea-surface temperature (SST) anomaly off the west coast of Tasmania (*9, 10*) that presumably contributed to reduced air temperatures over the island and reduced tree growth at other subalpine sites on the island (*11*). Growth has been unusually rapid since 1965 and parallels recent temperature increases in New Zealand (*8*), warm SSTs around Tasmania (*10*), and increased warming throughout much of the Southern Hemisphere (*12, 13*).

These apparent temperature changes were statistically modeled by comparing the huon

E. Cook, B. Buckley, R. D'Arrigo, Tree-Ring Laboratory, Lamont-Doherty Geological Observatory, Palisades, NY 10964.
T. Bird, Tasmanian Trades and Labour Council, Forestry Unit, New Town, Tasmania 7008, Australia.
M. Peterson, Tasmania Forestry Commission, Hobart, Tasmania 7001, Australia.
M. Barbetti, N. W. G. Macintosh Centre, University of Sydney, New South Wales 2006, Australia.
R. Francey, Commonwealth Scientific and Industrial Research Organization (CSIRO), Division of Atmospheric Research, Mordialloc, Victoria 3195, Australia.
P. Tans, Climate Monitoring and Diagnostics Laboratory, National Oceanic and Atmospheric Administration, Boulder, Colorado 80309.